Miner Petrol (2016) 110:361–377
DOI 10.1007/s00710-015-0392-4

ORIGINAL PAPER

Calcite and dolomite in intrusive carbonatites. II. Trace-element variations

Anton R. Chakhmouradian[1] · **Ekaterina P. Reguir**[1] · **Christopher Couëslan**[2] · **Panseok Yang**[1]

Received: 6 November 2014 / Accepted: 3 June 2015 / Published online: 16 June 2015

Abstract The composition of calcite and dolomite from several carbonatite complexes (including a large set of petrographically diverse samples from the Aley complex in Canada) was studied by electron-microprobe analysis and laser-ablation inductively-coupled-plasma mass-spectrometry to identify the extent of substitution of rare-earth and other trace elements in these minerals and the effects of different igneous and postmagmatic processes on their composition. Analysis of the newly acquired and published data shows that the contents of rare-earth elements (REE) and certain REE ratios in magmatic calcite and dolomite are controlled by crystal fractionation of fluorapatite, monazite and, possibly, other minerals. Enrichment in REE observed in some samples (up to ~2000 ppm in calcite) cannot be accounted for by coupled substitutions involving Na, P or As. At Aley, the REE abundances and chondrite-normalized $(La/Yb)_{cn}$ ratios in carbonates decrease with progressive fractionation. Sequestration of heavy REE from carbonatitic magma by calcic garnet may be responsible for a steeply sloping "exponential" pattern and lowered Ce/Ce* ratios of calcite from Magnet Cove (USA) and other localities. Alternatively, the low levels of Ce and Mn in these samples could result from preferential removal of these elements by Ce^{4+}- and Mn^{3+}-bearing minerals (such as cerianite and spinels) at increasing $f(O_2)$ in the magma. The distribution of large-ion lithophile elements (LILE = Sr, Ba and Pb) in rock-forming carbonates also shows trends indicative of crystal fractionation effects (e.g., concomitant depletion in Ba + Pb at Aley, or Sr + Ba at Kerimasi), although the phases responsible for these variations cannot be identified unambiguously at present. Overall, element ratios sensitive to the redox state of the magma and its complexing characteristics (Eu/Eu*, Ce/Ce* and Y/Ho) are least variable and in both primary calcite and dolomite, approach the average chondritic values. In consanguineous rocks, calcite invariably has higher REE and LILE levels than dolomite. Hydrothermal reworking of carbonatites does not produce a unique geochemical fingerprint, leading instead to a variety of evolutionary trends that range from light-REE and LILE enrichment (Turiy Mys, Russia) to heavy-REE enrichment and LILE depletion (Bear Lodge, USA). These differences clearly attest to variations in the chemistry of carbonatitic fluids and, consequently, their ability to mobilize specific trace elements from earlier-crystallized minerals. An important telltale indicator of hydrothermal reworking is deviation from the primary, chondrite-like REE ratios (in particular, Y/Ho and Eu/Eu*), accompanied by a variety of other compositional changes depending on the redox state of the fluid (e.g., depletion of carbonates in Mn owing to its oxidation and sequestration by secondary oxides). The effect of supergene processes was studied on a single sample from Bear Lodge, which shows extreme depletion in Mn and Ce (both due to oxidation), coupled with enrichment in Pb and U, possibly reflecting an increased availability of Pb^{2+} and $(UO_2)^{2+}$ species in the system. On the basis of these findings, several avenues for future research can be outlined: (1) structural mechanisms of REE uptake by carbonates; (2) partitioning of REE and LILE between cogenetic calcite and dolomite; (3) the effects of

Editorial handling: L. G. Gwalani

Electronic supplementary material The online version of this article (doi:10.1007/s00710-015-0392-4) contains supplementary material, which is available to authorized users.

✉ Anton R. Chakhmouradian
chakhmou@cc.umanitoba.ca

[1] Department of Geological Sciences, University of Manitoba, Winnipeg, MB R3T 2N2, Canada

[2] Manitoba Innovation, Energy and Mines, Manitoba Geological Survey, Winnipeg, MB R3G 3P2, Canada

fluorapatite, phlogopite and pyrochlore fractionation on the LILE budget of magmatic carbonates; (4) the cause(s) of coupled Mn-Ce depletion in some primary calcite; and (5) relations between fluid chemistry and compositional changes in hydrothermal carbonates.

Introduction

The existence of igneous carbonate(-bearing) rocks was initially postulated on the basis of field and petrographic observations at Kavant, India (Bose 1884; see also Sukheswala and Avasia 1971), Alnö, Sweden (Högbom 1895) and Kasaan Peninsula, Alaska (Wright 1915). These ideas were formalized by Brøgger (1921), who studied calcite- and dolomite-dominant dikes at Fen (Norway), compiled a large volume of data for similar occurrences elsewhere, and proposed the term *Karbonatite* to describe these unusual rocks of inferred magmatic origin. The International Union of Geological Sciences advocates restricting the term *carbonatite* to igneous rocks comprising >50 % modal carbonate, and referring to their silicate-rich counterparts as *silicocarbonatites* (SiO_2 > 20 wt.%), *carbonatitic* (10–50 % modal carbonate) or *carbonate-bearing* (<10 %) varieties of silicate rock types (Le Maitre 2002, p. 10). We agree with Mitchell (2005) that these divisions are artificial and serve no practical purpose whatsoever because carbonatites commonly show dramatic variations in modal composition, grading from anchimonomineralic calcitic or dolomitic rocks into cogenetic carbonate-bearing "ultramafic", "syenitic", etc. rocks on small spatial scales. We also recognize that most carbonatites were affected by hydrothermal processes at one time or another and, hence, are not exclusively igneous in origin (Chakhmouradian and Zaitsev 2012; Chakhmouradian et al. 2015a).

Carbonate minerals are the principal constituent of intrusive carbonatites, where their content exceeds 90 % in some rocks interpreted as cumulates (Xu et al. 2007). In order to understand the role of these minerals in carbonatite evolution and in the distribution of specific trace elements among different carbonatite facies, it is essential to know the extent to which these elements can be incorporated in rock-forming carbonates and those factors that control their uptake. Without this knowledge, it is impossible to interpret correctly much of petrologic data used routinely for tracking the origin of carbonatitic magmas (e.g., radiogenic isotope ratios, or textural interrelations between silicate and carbonate minerals). This information is also important from a practical standpoint: for example for the study of igneous and hydrothermal rare-earth deposits associated with carbonatites (Xu et al. 2008a, 2010). Despite all this, there is a limited amount of published data on the trace-element chemistry of carbonate minerals from igneous rocks. In many cases, the reported contents of such heavy elements as Ba or lanthanides were measured by electron-microprobe analysis (EMPA), but cannot be considered reliable because their detection limits were not specified (Currie et al. 1992). The present contribution summarizes the trace-element information available in the literature, provides new data for several occurrences not studied by previous workers, and puts some principal observations that stem from this combined geochemical evidence in the context of carbonatite petrogenesis.

Background information

The present work focuses on calcite and dolomite because these minerals account for the bulk of igneous carbonate material. Calcite is a trigonal $CaCO_3$ polymorph (Markgraf and Reeder 1985; Table 1) that at ambient conditions, forms only limited solid solutions with isostructural Mg, Mn and Fe^{2+} carbonates, and aragonite-type orthorhombic $SrCO_3$, $BaCO_3$ and $PbCO_3$ (Chang and Brice 1972; Brice and Chang 1973; De Capitani and Peters 1981; Anovitz and Essene 1987). The limited miscibility between $CaCO_3$ and $MgCO_3$ ($FeCO_3$) explains the existence of cation-ordered structures along the $Ca(Mg,Fe)(CO_3)_2$ join, which is incomplete for reasons poorly understood at present (Reeder and Dollase 1989). These structures cover a wide compositional range from pure dolomite to ~23 wt.% FeO or 70 mol% $CaFe(CO_3)_2$, i.e. approach the solubility limit established for these minerals empirically (ibid.; Table 1). However, ankerite-dominant carbonates (>18 wt.% FeO) appear to be restricted to late-stage postmagmatic parageneses (Chakhmouradian et al. 2015a). In both calcite and dolomite, the divalent cations are coordinated by six atoms of oxygen, but the Ca site is more spacious in the latter, which accounts for complete miscibility between $CaMg(CO_3)_2$ and $SrMg(CO_3)_2$ in synthetic systems, but only limited incorporation of Sr in calcite (Brice and Chang 1973). At 650 °C and 5 bar, the miscibility gap is delineated by Sr-rich dolomite $(Ca_{0.72}Sr_{0.28})Mg(CO_3)_2$, calcite $(Ca_{0.80}Sr_{0.12}Mg_{0.08})CO_3$ and Ca-rich strontianite $(Sr_{0.57}Ca_{0.40}Mg_{0.03})CO_3$ (ibid.); note that under experimental conditions, equilibrated dolomite and calcite appear to have comparable Sr contents.

The incorporation of non-divalent cations in rock-forming carbonates is problematic because it requires coupled substitutions in proximal sites to avoid under- or overbonding of oxygens in carbonate groups. For example, the replacement of two Ca^{2+} ions by similarly-sized Na^{+} and REE^{3+} can be envisioned to occur where these elements are readily available (e.g., in carbonatites). Correlation of Na and REE partition coefficients between calcite and aqueous solutions has been documented by Zhong and Mucci (1995). In practice, however, this substitution will be very limited owing to structural strain that it creates. Carbonates of the type $NaREE(CO_3)_2$ do exist, but differ structurally from calcite (Schweer and Seidel 1981), in part owing to the affinity of REE^{3+} ions for

Table 1 Calcite and dolomite: a summary of crystal chemistry from the literature

Calcite, $CaCO_3$		Dolomite-ankerite, $Ca(Mg,Fe)(CO_3)_2$	
Crystallographic details for 24 °C [1]:		Crystallographic details for 24 °C [2,3]:	
Crystal system	Trigonal	Crystal system	Trigonal
Space group	R-$\bar{3}$c	Space group	R-$\bar{3}$
a	4.988(1) Å	*a*[a]	4.8116–4.8312 Å
c	17.061(1) Å	*c*[a]	16.020–16.1663 Å
Ca-O distance	2.3595(5) Å	Ca-O distance[a]	2.3822–2.3716 Å
		Mg/Fe-O distance[a]	2.0821–2.1266 Å
Maximum reported contents of selected substituent elements (carbonatites):		Maximum reported contents of selected substituent elements (carbonatites):	
Na	751 ppm [4]	Na	155 ppm [4]
MgO	4.31 wt.% [5]		
MnO	5.69 wt.% [6]	MnO	3.55 wt.% MnO [16]
FeO	4.99 wt.% [7]		
SrO	13.1 wt.% [8]	SrO	3.88 wt.% [6]
Y	547 ppm [9]	Y	307 ppm [17]
BaO	2.20 wt.% [10]	Ba	242 ppm [18]
Ln[b]	2308 ppm [11]	Ln[b]	651 ppm [19]
Selected element ratios (range):		Selected element ratios (range):	
Y/Ho	18.4 [12]–46.2 [13]	Y/Ho	12.4 [12]–39.5 [20]
$(La/Yb)_{cn}$	0.05 [14]–528 [15]	$(La/Yb)_{cn}$	2.4 [14]–241 [12]

[a] Given in order of increasing Fe content to ~70 mol% $CaFe(CO_3)_2$

[b] Lanthanides only

References

[1] Markgraf and Reeder (1985); [2] Effenberger et al. (1981); [3] Reeder and Dollase (1989); [4] Phalaborwa (Dawson and Hinton 2003), but EMPA measurements give much higher values, i.e. up to 0.76 wt.% Na_2O in calcite from altered natrocarbonatite, Oldoinyo Lengai, Tanzania (Keller and Zaitsev 2006); [5] Goldray, Canada (Chakhmouradian et al. 2015a); [6] Khibiny, Russia (Zaitsev 1996); [7] Mud Tank, Australia (Currie et al. 1992); [8] Sarnu Dandali, India (Wall et al. 1993); [9] Huanglongpu, China (Xu et al. 2007); [10] Murun, Russia (Konev et al. 1996); [11] Phalaborwa, South Africa (Dawson and Hinton 2003); a value of 3827 ppm was cited by Hornig-Kjarsgaard (1998) in Table 5, but appears to be a typo; 3030 ppm REE, reported by Ionov and Harmer (2002), clearly comes from a contaminated analysis and was discarded; [12] ibid.; [13] Daluxiang, China (Xu et al. 2008b); [14] Spitskop, South Africa (Ionov and Harmer 2002); [15] Kaiserstuhl, Germany (Hornig-Kjarsgaard 1998); [16] Kangankunde, Malawi (Buckley and Woolley 1990); values up to 21.52 wt.% were reported for ternary kutnohorite-dolomite-ankerite compositions in [6]; [17] Wekusko Lake, Canada (Chakhmouradian et al. 2009); [18] ibid., but EMPA measurements give much higher values, i.e. up to 0.27 wt.% BaO was reported in [7]; [19] the actual total of lanthanide abundances for analysis Fe1b from Fen, Norway, for which Hornig-Kjarsgaard (1998) cited 442 ppm REE; [20] Siilinjarvi, Finland (Hornig-Kjarsgaard 1998)

coordination numbers higher than six (e.g., Grice et al., 2000a, b). Although replacement of carbonate groups by $(HCO_3)^-$ ions could facilitate the uptake of monovalent cations, protonation is essentially limited to the reactive near-surface layer (Villegas-Jiménez et al. 2009) and is unlikely to account for several thousand ppm Na measured by EMPA in some studies (Table 1, footnote). Alternatively, the uptake of rare earths could be facilitated by anionic substitutions (Alexandratos et al. 2007), such as $Ca^{2+} + (CO_3)^{2-} = REE^{3+} + [(P,As)O_4]^{3-}$. Up to ~300 ppm As can be incorporated in the growth layer of calcite crystals experimentally (ibid.), but it is unclear whether such high levels of tetrahedrally coordinated As and P can be retained on the bulk scale. Obviously, the incorporation of large tetravalent cations (Zr, Th and U) will create an even more imbalanced distribution of bond valence and, hence, be less likely to occur. Indeed, these elements are given as below detection (<<1 ppm) in most published analyses, although values in excess of 1 ppm Th or Zr and 0.5 ppm U have been reported in some studies (e.g., Xu et al. 2010).

In addition to their absolute abundances, the knowledge of the *relative enrichment or depletion* of certain trace elements with respect to other substituents in the same mineral is important for tracking the processes of magma and fluid evolution. For this purpose, geochemists typically use mass ratios that reflect fractionation between, or within a group of, elements whose partitioning behavior is sensitive to changes in the physicochemical properties of the system. These ratios are calculated either from the analytically determined concentrations of individual elements, or from concentrations normalized to some standard set of values (e.g., the composition of an average CI carbonaceous chondrite). The most widely used ratio is $(La/Yb)_{cn}$, replaced in some studies by $(La/Lu)_{cn}$

(where the subscript indicates chondrite normalization), both of which are essentially a measure of separation between light REE (LREE = La-Eu) and heavy REE (HREE = Gd-Lu) in response to various evolutionary processes (e.g., precipitation of minerals favoring one of these element groups over the other). Other conventionally used ratios are Ce/Ce* and Eu/Eu*, which reflect deviation of the measured Ce and Eu concentrations, respectively, from the values interpolated from the abundances of their neighboring lanthanides: $Ce/Ce^* = Ce_{cn}/(0.5La_{cn} + 0.5Pr_{cn})$, $Eu/Eu^* = Eu_{cn}/(0.5Sm_{cn} + 0.5Gd_{cn})$. Both these ratios are sensitive to the redox state of the system. For example, Ce can be oxidized to Ce^{4+} and scavenged by low-solubility minerals, such as cerianite (CeO_2) and Fe^{3+}-Mn^{4+} (hydr)oxides, thereby reducing the Ce/Ce* value of the residual liquid, commonly expressed as a negative Ce anomaly ($0 < Ce/Ce^* < 1$) in chondrite-normalized REE distribution patterns of minerals associated with cerianite and secondary (hydr)oxides (Ohta and Kawabe 2001; Bühn et al. 2003; Bau and Koschinsky 2009; Moore et al. 2015). Europium speciation and partitioning are affected by its (partial) reduction to Eu^{2+}, which results in positive Eu anomalies ($Eu/Eu^* > 1$) in materials preferentially incorporating the larger Eu^{2+} cation and complementary negative anomalies in those accommodating trivalent lanthanides (Douville et al. 2002; Eickmann et al. 2009). Finally, the Y/Ho value is a measure of decoupling between these two very similar elements, documented in some volatile-rich igneous and hydrothermal systems (for possible mechanisms driving this decoupling, see Bühn et al. 2003; Bau and Koschinsky 2009; Chakhmouradian et al. 2013). Further discussion of trace-element ratios and their applicability to petrogenetic research is beyond the scope of the present work; interested readers are addressed to the voluminous geochemical literature on this subject.

Methods

In order to determine trace-element variations in igneous carbonates, we examined a large suite of genetically related samples representing the entire diversity of carbonatite types from the Aley intrusive complex in British Columbia, Canada (Chakhmouradian et al. 2015b). Calcite and dolomite from 20 to 35 samples, respectively, were analyzed using EMPA and laser-ablation inductively-coupled-plasma mass-spectrometry (LA-ICPMS). The same methods were then used to quantify the composition of calcite from Turiy Mys (Russia), Kerimasi (Tanzania), Magnet Cove and Bear Lodge (USA), Prairie Lake, Cinder Lake and Paint Lake (Canada), and dolomite from Upper Fir and Paint Lake (Canada). Detailed sample descriptions are provided in electronic Appendix 1. Energy-dispersive spectrometry in combination with polarized-light and back-scattered electron (BSE) imaging was used for the selection of areas for quantitative analysis. The concentrations of Mg, Ca, Mn and Fe were determined by wavelength-dispersive spectrometry (WDS) using a Cameca SX 100 automated electron microprobe operated at 15 kV and 10 nA with a 10 μm beam. The following natural standards were employed in the analysis: forsterite (Mg), diopside (Ca), spessartine (Mn), fayalite (Fe); the $K\alpha$ lines were used for all of these elements. Typical detection limits are 300–400 ppm for Mg, 200–300 ppm for Ca, and 600–700 ppm for Mn and Fe. Phosphorus (calibrated using a fluorapatite standard) was found not to be present in concentrations above its lower detection limit by WDS (~130 ppm) in any of the calcite or dolomite, including the most REE-rich samples (see below).

The abundances of selected trace elements were measured by LA-ICPMS using a 213-nm Nd-YAG Merchantek laser connected to a Thermo Finnigan Element 2 sector-field mass-spectrometer. The trace-element compositions were obtained using spot analyses of calcite and dolomite grains in polished "thick" sections (~100 μm in thickness) using matching BSE, transmitted- and reflected-light images of the areas analyzed by WDS to accurately position a laser beam on the sample and ensure that only inclusion-free areas unaffected by fracturing or alteration were ablated. The laser beam size varied from 30 to 40 μm, with laser-energy density ranging from 4.9 to 6.15 J/cm^2 at a repetition rate of 10 Hz. Ablation was done in Ar and He atmospheres. All analyses were performed in a low-resolution mode (~300) using Pt skimmer and sample cones. Synthetic glass standard NIST SRM 610 was employed for calibration and quality control. Data reduction was carried out online using the GLITTER software (van Achterbergh et al. 2001). The Ca content measured by WDS was used as an internal standard for all analyses. The quality control was achieved by keeping the fractionation at less than 10 % and fractionation/error ratio at <3. The maximum abundances and detection limits for all analyzed trace elements are summarized in Table 2. Selected LA-ICPMS data are given in Tables 3, 4 and Appendix 2. All element ratios discussed below are based on mass abundances; where applicable, chondrite normalization values are from Anders and Grevesse (1989).

Results and discussion

Aley carbonatite complex

The material from Aley represents primary calcite and dolomite (Fig. 1a–d), dolomite developed at the expense of primary calcite (Fig. 1e), and late-stage hydrothermal dolomite confined to fractures and vugs (Fig. 1f). These paragenetic interpretations were made on the basis of the morphological characteristics and textural interrelations of the carbonate minerals; for further details, see Chakhmouradian et al. (2015a, 2015b).

Table 2 Calcite and dolomite: a summary of maximum trace-element abundances (this work)

Calcite, $CaCO_3$			Dolomite-ankerite, $Ca(Mg,Fe)(CO_3)_2$		
Potential Ca substituents (ppm):			Potential Ca/Mg/Fe substituents (ppm):		
	Abundance	Detection limit		Abundance	Detection limit
Na	734[a]	40–60	Na	<14	10–14
Sc	10.0	0.16–0.25	Sc	31	0.06–0.25
V	0.10[a]	0.04–0.18	V	50	0.05–0.07
Mn	4815	0.10–0.33	Mn	13,511	0.08–0.18
Rb	0[a]	0.03–0.11	Rb	0.08[a]	0.03–0.06
Sr	21,229	0.57–2.40	Sr	6977	0.58–0.79
Y	157	0.008–0.06	Y	89	0.008–0.03
Cd	0.55	0.22–0.47	Cd	2.8	0.08–0.33
Ba	2151	0.19–0.41	Ba	597	0.09–0.28
LREE[b]	1685	≤0.11 (Sm)	LREE[b]	248	≤0.07 (Nd)
HREE[b]	111	≤0.94 (Gd)	HREE[b]	60	≤0.29 (Gd)
Pb	370	0.007–0.04	Pb	3.0	0.008–0.015
Th	5.6	0.003–0.017	Th	12	0.003–0.008
U	2.3	0.008–0.04	U	0.58	0.009–0.014
Potential C substituents (ppm):			Potential C substituents (ppm):		
	Abundance	Detection limit		Abundance	Detection limit
P	<130	100–130	P	<130	100–130
As	1.4	0.15–0.35	As	1.9	0.08–0.23
Se	3.7	1.3–2.8	Se	5.8	0.7–1.7

[a] For those elements, whose maximum and third largest values differ by > 60 % of the maximum value, the 75th percentile is given instead

[b] LREE = La–Eu; HREE = Gd–Lu

The abundances of Mg, Mn, Sr, Ba, REE and Pb in the primary calcite consistently exceed their detection limits by LA-ICPMS, but range over one order of magnitude or more (Table 3). The content of U is consistently at or below its lower limit of detection, whereas 91 % of the recorded Th values are <1 ppm. Relatively high Th values (up to 5.6 ppm) in a few analyses likely result from contamination by submicroscopic inclusions of Th-rich minerals. The only meaningful, yet weak, correlations observed are those between the abundances of LREE, Ba and Pb (Fig. 2a and b). Some element ratios (Y/Ho, Ce/Ce* and Eu/Eu*) show remarkably little variation across the entire sample suite (Fig. 2c), whereas other ratios – notably $(La/Yb)_{cn}$ – are extremely variable (1.7–84). There is a good correlation (R^2=0.69) between the $(La/Yb)_{cn}$ and total REE values (Fig. 2d). Removing the outliers representing a single sample (AL3A), which form their own distinct trend (see below), gives a much better R^2 value of 0.89.

The primary dolomite from Aley is difficult to distinguish from the products of calcite dolomitization on the basis of their trace-element abundances, principally because of the wide compositional variations in the precursor calcite (see above) and ambiguity of textural relations between calcite and dolomite in some of the samples (cf. Fig. 1d and e). Note, however, that pervasively dolomitized carbonatites show a distinct C-O signature indicative of a heavy-isotope crustal input (Chakhmouradian et al. 2015b). Both varieties exhibit a significant variation in the content of Sr, Ba, REE and Pb, but are poorer in these elements than most of the calcite (cf. Tables 3 and 4; Fig. 1d and e). In common with the latter, the highest Ba contents recorded in the dolomite are generally associated with enrichment in LREE and Pb, but there is essentially no correlation among the different samples (Fig. 2e and f). In Fig. 2d, there appears to be a positive correlation trend toward higher $(La/Yb)_{cn}$ values than in the calcite (0.8–303), although a significant number of data points corresponding to dolomitized calcite (e.g., Fig. 1e) plot at the low-REE end of the calcite cluster at $(La/Yb)_{cn} < 20$. The average Y/Ho, Eu/Eu* and Ce/Ce* ratios are indistinguishable in both dolomite varieties and are close to, but show more scatter than, the calcite values (Fig. 2c).

Primary magmatic calcite and dolomite outside of Aley

The calcite samples from Kerimasi, Magnet Cove, Prairie Lake, Cinder Lake and Paint Lake, and the dolomite sample from Upper Fir can be interpreted as primary magmatic carbonates lacking any evidence of subsolidus chemical re-equilibration (Chakhmouradian et al. 2015a). In general, their trace-element abundances and ratios are within the limits established for these minerals in the previous studies

Table 3 Trace-element composition of calcite from carbonatites: mean values (number of LA-ICPMS spot analyses), estimated standard deviations (ESD) and selected spot analyses (Aley data only)

ppm	Turiy Mys		Kerimasi		Magnet Cove		Bear Lodge, hydr.		Bear Lodge, superg.	
	Mean (8)	ESD	Mean (9)	ESD	Mean (8)	ESD	Mean (6)	ESD	Mean (4)	ESD
Mg	59	11	864	198	165	19	202	11	630	36
Mn	540	31	33	20	75	9	717	36	b.d.	b.d.
Sr	19,776	1114	1563	833	6037	228	57	3	712	87
Y	5.1	0.8	31	11	3.5	0.5	64	4	8.5	2.8
Ba	706	64	499	294	289	43	0.15	0.07	2.5	0.1
La	322	20	131	42	43	6	1.7	0.2	87	38
Ce	404	20	130	60	29	5	4.9	0.4	7.7	3.7
Pr	32	1	15	5	1.8	0.4	0.88	0.06	15	5
Nd	88	3	55	16	5.0	0.8	5.7	0.3	57	18
Sm	5.8	0.7	8.7	2.7	0.94	0.31	2.2	0.2	10	3
Eu	1.2	0.2	2.7	0.9	0.29	0.11	1.31	0.03	2.4	0.6
Gd	3.0	0.4	8.0	2.6	b.d.	b.d.	4.1	0.4	6.2	1.6
Tb	0.24	0.06	1.2	0.4	b.d.	b.d.	0.69	0.03	0.49	0.13
Dy	0.95	0.16	5.8	2.1	0.76	0.02	5.2	0.2	1.6	0.5
Ho	0.12	0.03	1.1	0.4	0.11	0.02	1.6	0.1	0.25	0.07
Er	0.30	0.08	3.0	1.0	0.28	0.05	5.4	0.3	0.47	0.15
Tm	0.06	0.01	0.42	0.23	b.d.	b.d.	0.79	0.06	0.05	0.01
Yb	0.27	0.13	2/3	0.9	b.d.	b.d.	5.2	0.3	0.28	0.09
Lu	0.06	0.01	0.43	0.22	b.d.	b.d.	0.81	0.08	0.05	0.02
ppm	Cinder Lake		Prairie Lake		Paint Lake		Aley			
	Mean (4)	ESD	Mean (5)	ESD	Mean (8)	ESD	1	2	3	4
Mg	2549	881	3445	3006	2791	76	5755	13,148	707	7100
Mn	3801	347	1044	920	1101	26	4815	2576	2132	2086
Sr	6137	3342	4863	147	3897	61	8433	8242	4581	10,767
Y	104	15	67	2	108	2	87	82	71	67
Ba	7.3	3.4	36	13	38	6	1752	1908	2151	732
La	31	7	199	11	43	3	457	403	319	356
Ce	126	24	371	24	128	6	752	699	506	575
Pr	22	4	44	3	22	1	89	62	52	56
Nd	130	27	186	12	134	5	324	209	178	198
Sm	40	7	31	1	36	1	49	28	29	30
Eu	14	2	10.1	0.4	11.1	0.2	15	12	8.9	8.3
Gd	37	7	26	3	34	0.9	35	32	21	22
Tb	3.6	0.5	3.2	0.4	4.4	0.2	4.1	3.5	2.6	2.6
Dy	21	4	16	2	20.8	0.4	19	18	15	13.9
Ho	3.6	0.7	2.8	0.2	3.7	0.2	3.4	3.1	2.6	2.4
Er	7.7	1.5	5.9	0.8	8.3	0.4	7.2	9.0	6.7	6.2
Tm	1.0	0.2	0.7	0.1	1.1	0.1	0.94	0.90	0.98	0.79
Yb	5.2	1.6	3.9	0.6	6.8	0.5	5.7	6.1	4.9	5.4
Lu	0.6	0.2	0.62	0.11	1.0	0.1	0.86	0.78	0.59	0.77

b.d. below detection (see Table 2 or details)

(Hornig-Kjarsgaard 1998; Dawson and Hinton 2003; Xu et al. 2007, 2008a, b, 2010; Chakhmouradian et al. 2009; Faiziev and Gafurov 2010; Zaitsev et al. 2014). The only exception is small deficiency of Ce in the Kerimasi and Magnet Cove calcite, such that most of the analyses show La > Ce and the Ce/Ce* values ranging from 0.40 to 0.79 and 0.53, respectively. The resultant chondrite-normalized REE patterns do not show a trough at Ce, as one might expect, but have a peculiar "exponential" shape with a steep drop from La to Sm, followed by a more gentle decline toward heavier lanthanides (Fig. 3a).

Table 4 Trace-element composition of dolomite from carbonatites: mean values (number of LA-ICPMS spot analyses), estimated standard deviations(ESD) and selected spot analyses (Aley data only)

ppm	Upper Fir		Paint Lake		Aley		
	Mean (16)	ESD	Mean (8)	ESD	1	2	3
Mg	91,391	3663	105,443	1866	98,765	78,290	71,029
Mn	7817	233	2451	23	13,511	2802	2663
Sr	4745	142	2363	29	1694	6977	6155
Y	9.2	1.6	2.5	0.3	6.6	9.9	33
Ba	57	6	2.7	0.1	60	138	598
La	45	8	5.2	0.5	3.8	18	46
Ce	81	13	17	1	14	38	105
Pr	8.4	1.5	2.7	0.3	2.1	4.7	13
Nd	32	5	13	1	9.3	20	60
Sm	5.1	1.0	2.7	0.5	2.9	5.3	15
Eu	1.5	0.2	1.3	0.1	1.2	2.1	4.1
Gd	3.7	0.7	1.9	0.5	2.1	4.9	12
Tb	0.45	0.08	0.21	0.08	0.30	0.67	1.7
Dy	2.2	0.3	0.73	0.09	2.1	2.5	8.0
Ho	0.38	0.05	0.09	0.02	0.29	0.37	1.2
Er	0.89	0.13	0.24	0.06	0.59	0.70	2.5
Tm	0.11	0.02	0.03	0.01	0.07	0.11	0.33
Yb	0.69	0.11	0.16	0.03	0.40	0.62	1.9
Lu	0.10	0.02	0.04	0.01	0.11	0.07	0.25

Hydrothermal carbonates

One of the Aley carbonatites contains fractures lined with rhombohedral crystals of hydrothermal dolomite (Dol 3 in Fig. 1f), whose rim is characterized by higher Mg and REE, but lower Mn, Fe, Sr and Ba levels in comparison with the earlier-crystallized massive variety in the same sample (Dol1). The intermediate zone of dolomite crystals (Dol2) is transitional in composition. The Y/Ho and Ce/Ce* values are within the estimated standard deviation in the euhedral and massive varieties (24±6 vs. 21±5 and 0.96±0.27 vs. 0.88±0.11, respectively), whereas their Eu/Eu* ratio could not be quantified because Gd is below its detection limit by LA-ICPMS in all analyses. The depletion of the hydrothermal crystals in Sr and Mn (≤1100 and 2500 ppm, respectively) clearly sets them apart from the rest of the Aley dolomite (Fig. 3b). These differences are further amplified in the plot of Mg/Mn vs. Eu/Sr (Fig. 3c), where the early-crystallizing and hydrothermal carbonates plot as discrete fields. The Mn-Fe depletion was undoubtedly caused by oxidation of both elements during interaction of the carbonatite with a fluid, as indicated by the abundance of pseudomorphs of Mn-bearing goethite ($Fe^{3+}OOH$ with 3300–3800 ppm Mn) after pyrite in this sample. The Eu/Sr ratio, plotted along the abscissa, was chosen in preference to some other measure of REE enrichment relative to Sr depletion, because it can be used as a proxy for redox conditions in those cases where the Eu/Eu* value is unavailable. Given that the Eu^{2+} ion has the same radius as Sr^{2+} (Shannon 1976), the Eu/Sr value of carbonate minerals should be expected to decrease in a strongly oxidizing environment (see Late-stage calcite from Bear Lodge). In the Aley sample, the observed increase in Eu/Sr, coupled with the absence of any detectable Ce anomalies (cf. Fig. 3a and d), implies that the fluid that precipitated the rhombohedral dolomite and oxidized pyrite did not affect Eu or Ce.

The dolomite sample from Paint Lake is unusual in showing a consistent positive Eu anomaly (Eu/Eu*=1.7±0.2; Fig. 3d), while being otherwise compositionally unremarkable. Its Sr and REE contents, Y/Ho, Ce/Ce* and Mg/Mn ratios are well within the limits established for carbonatitic dolomite in the literature (Hornig-Kjarsgaard 1998; Dawson and Hinton 2003; Chakhmouradian et al. 2009; Zaitsev et al. 2014) and present work (Table 4). The published analyses give Eu/Eu* values ranging from 0.8 to 1.2, whereas the Aley and Upper Fir samples average 1.01±0.17 and 1.01±0.06, respectively. The Paint Lake carbonatite contains abundant clinochrysotile pseudomorphs after olivine, and it is feasible that the observed enrichment of dolomite in Eu was caused by the same hydrothermal process that brought about serpentinization. Carbonates deposited in a reducing hydrothermal environment (e.g., seafloor serpentinites) commonly exhibit a positive Eu anomaly (e.g., Eickmann et al. 2009) thought to arise from mobilization of Eu^{2+} from feldspars in the host rock, or differences in the complexing behavior of Eu^{2+} and Eu^{3+} (for discussion, see Douville et al. 2002). A detailed study of the Paint Lake occurrence is currently underway to examine the extent of hydrothermal overprint.

Calcite carbonatites from Turiy Mys and Bear Lodge also show evidence of hydrothermal alteration, both petrographic (e.g., zoning in fluorapatite crystals) and geochemical. The Turiy Mys sample has high Y/Ho, but low Eu/Eu* and Mg/Mn ratios (46±10, 0.80±0.09, 0.11±0.02, respectively) differing from typical magmatic calcite (cf. 22–32, 0.9–1.3 and 0.3–5.5 in the Aley samples). The Bear Lodge material is also characterized by high Y/Ho and low Mg/Mn values (40.4±0.8 and 0.28±0.02, respectively), but shows a slight positive Eu anomaly (Eu/Eu* = 1.3±0.1). Other significant differences between these samples include very low Sr, Ba and Pb levels in the Bear Lodge sample and its enrichment in HREE relative to LREE [$(La/Yb)_{cn}$ = 0.22±0.02], all in striking contrast to the high levels of large-ion lithophile cations and LREE [$(La/Yb)_{cn}$ = 478–1742] in the Turiy Mys calcite (Fig. 3a). The enrichment of the Bear Lodge material in Eu, coupled with its depletion in Sr, results in elevated Eu/Sr ratios (0.023±0.01), far exceeding those in unmodified magmatic calcite (≤0.005).

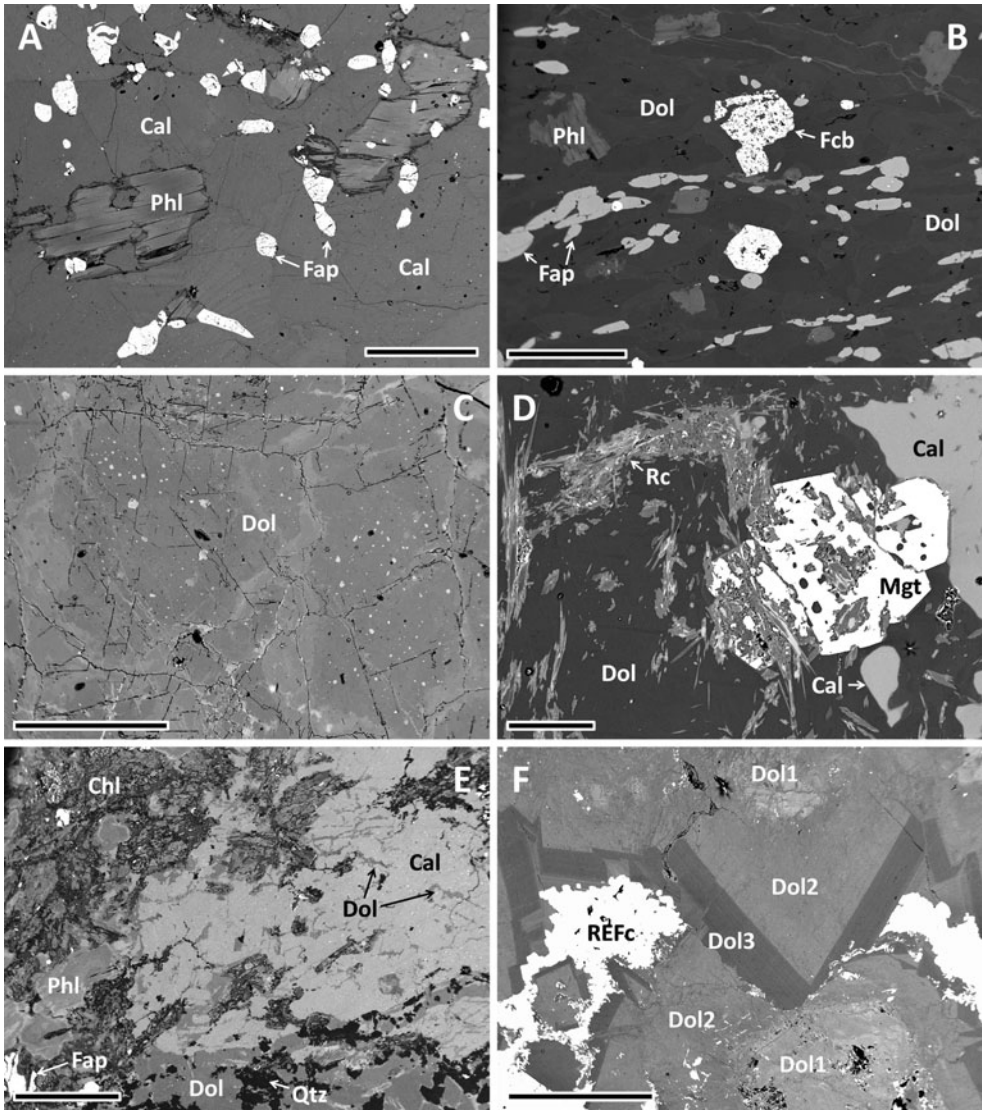

Fig. 1 Representative textural and paragenetic characteristics of calcite and dolomite from the Aley carbonatite complex, Canada. BSE images; *scale bar* is 0.5 mm for all images, except (**d**) (0.1 mm). **a** Primary calcite (Cal) associated with fluorapatite (Fap) and phlogopite (Phl) in calcite carbonatite (AL3A, see text); the calcite contains up to 6000 ppm Sr, 620 ppm Ba and 1050 ppm REE. **b** Primary dolomite (Dol) associated with fluorapatite, phlogopite and ferrocolumbite (Fcb) in dolomite carbonatite; the dolomite contains up to 5600 ppm Sr, 60 ppm Ba and 200 ppm REE. **c** Primary dolomite containing syngenetic inclusions of calcite; inclusion-free areas contain up to 4000 ppm Sr, 60 ppm Ba and 100 ppm REE. **d** Carbonatite consisting of relict calcite (5400–6300 ppm Sr, 450–570 ppm Ba, 320–430 ppm REE) and magnetite enclosed in dolomite (2200–2600 ppm Sr, 20–40 ppm Ba, 90–170 ppm REE) associated with richterite (Rc). **e** Primary calcite (up to 10,000 ppm Sr, 1750 ppm Ba, 1850 ppm REE) partially replaced by dolomite (up to 7000 ppm Sr, 600 ppm Ba, 300 ppm REE) along the margin and fractures; also present is chlorite (Chl) and quartz (Qtz). **f** Primary igneous dolomite (Dol1) resorbed and overgrown by euhedral hydrothermal dolomite (Dol2, Dol3) associated with rare-earth fluorocarbonates (REFc); the darker color of late-stage Dol reflects its lower Fe and Mn contents (see Hydrothermal carbonates)

Late-stage calcite from Bear Lodge

Calcite crystals from parts of the Bear Lodge deposit affected by oxidation (Moore et al. 2015) are notable for their extreme depletion in Mn (<0.12 ppm; Mg/Mn > 4875) and Ce (Ce/Ce* = 0.046±0.005), coupled with enrichment in Pb (286–370 ppm) and U (1.8–2.3 ppm) unparalleled by any other carbonatite sample described in the present work or literature. The intimate association of this calcite with Fe-Mn (hydr)oxides and cerianite indicates that these minerals represent a supergene paragenesis. In comparison with the

Fig. 2 Compositional variation of calcite (*black circles*) and dolomite (*grey diamonds*) from Aley, Canada. The Ce/Ce* and Eu/Eu* values calculated using the chondrite values of Anders and Grevesse (1989) and the following equations: $Ce/Ce^* = Ce_{cn}/(0.5La_{cn}+0.5Pr_{cn})$, $Eu/Eu^* = Eu_{cn}/(0.5Sm_{cn}+0.5Gd_{cn})$. These values and those obtained by geometric interpolation are well within the error of each other

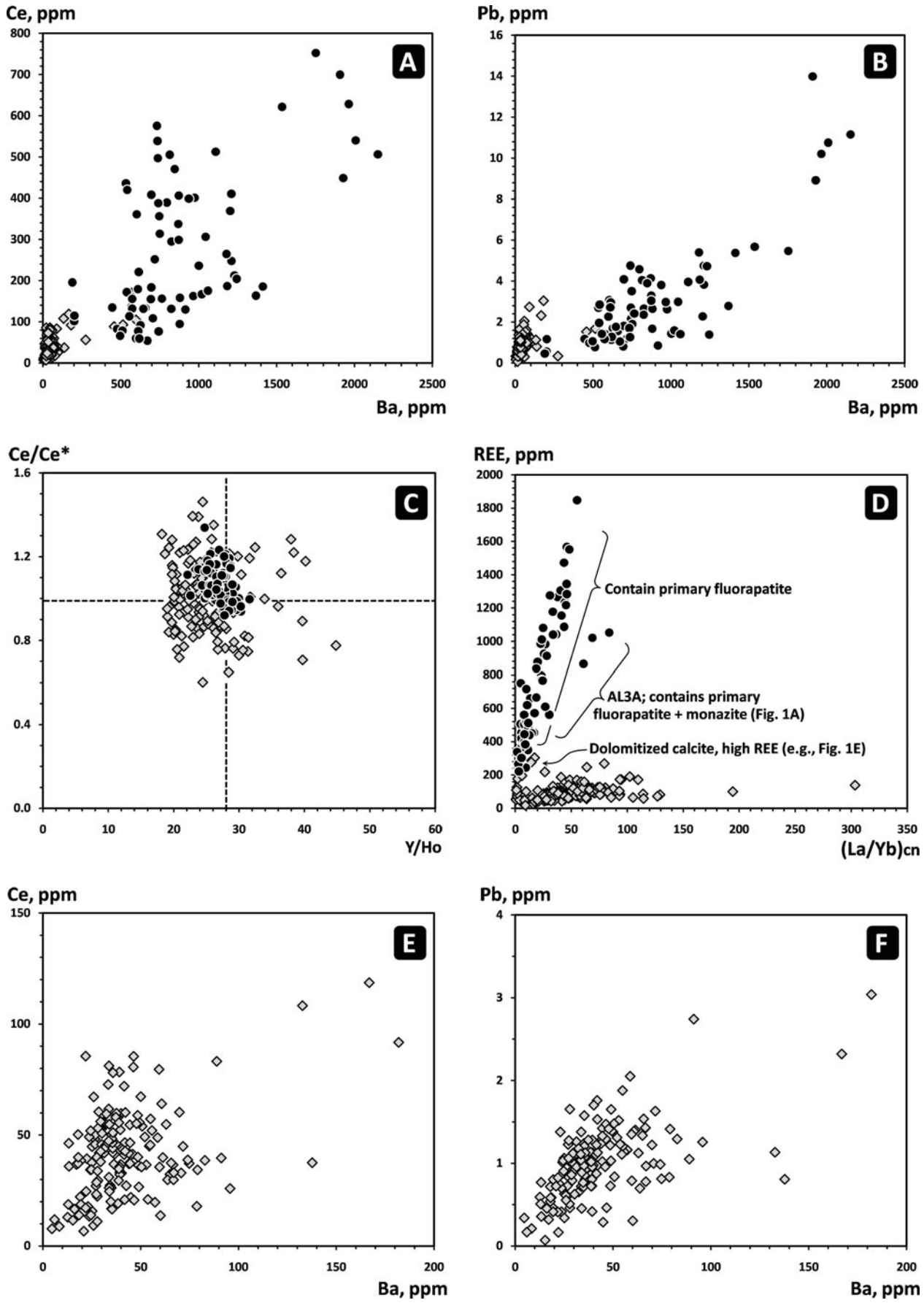
Ce, ppm
A
Ba, ppm
Pb, ppm
B
Ba, ppm
Ce/Ce*
C
Y/Ho
REE, ppm
D
Contain primary fluorapatite
AL3A; contains primary fluorapatite + monazite (Fig. 1A)
Dolomitized calcite, high REE (e.g., Fig. 1E)
(La/Yb)cn
Ce, ppm
E
Ba, ppm
Pb, ppm
F
Ba, ppm

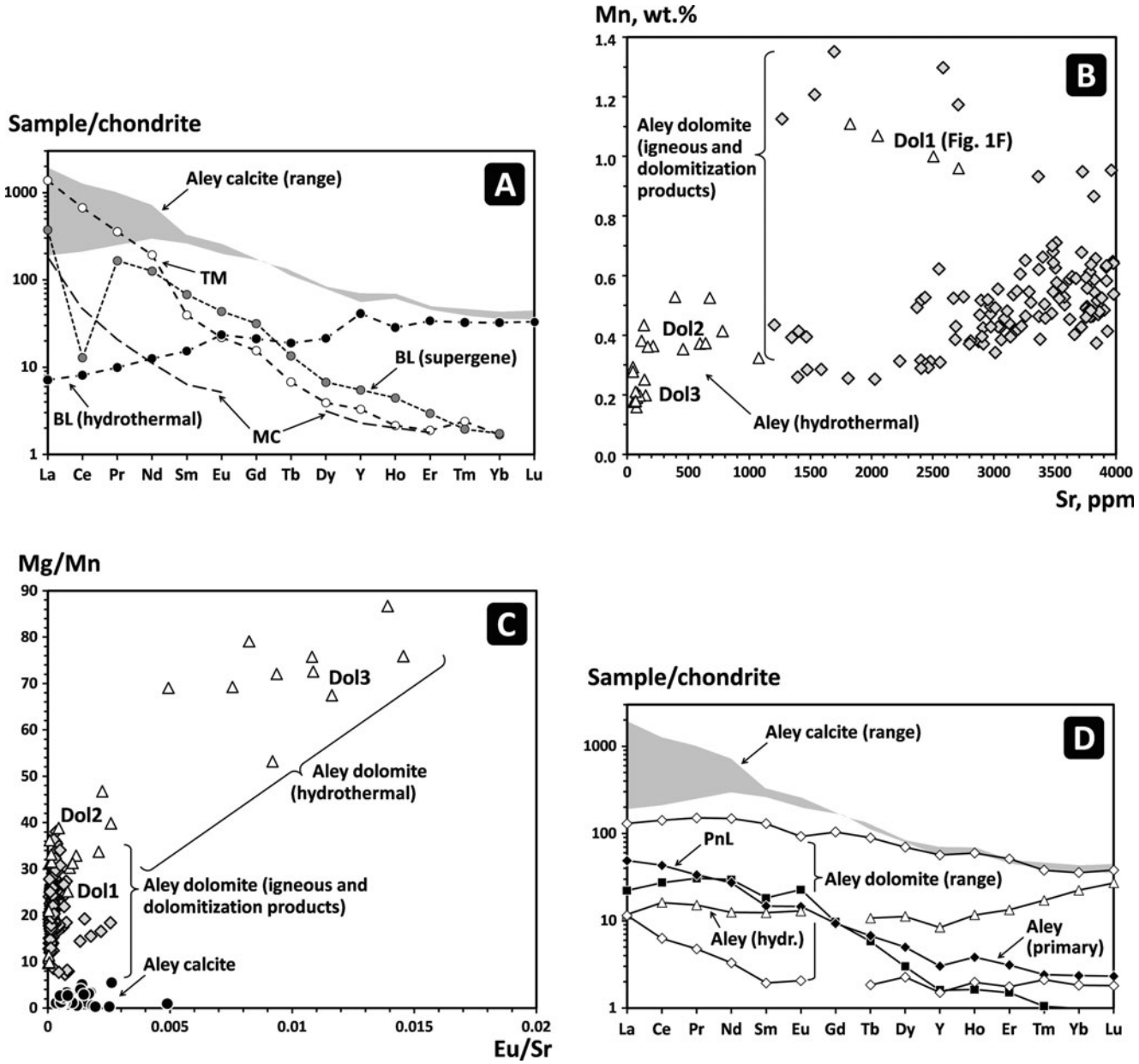

Fig. 3 Compositional variation of selected calcite and dolomite samples from Aley (*black circles* = calcite; *grey diamonds* = primary dolomite or products of calcite dolomitization; *empty triangles* = euhedral hydrothermal dolomite crystals from fractures), calcite from Bear Lodge (BL), Turiy Mys (TM), Magnet Cove (MC), and dolomite from Paint Lake (PnL). For (**a**) and (**d**), normalization values were taken from Anders and Grevesse (1989)

hydrothermally altered calcite from the same sample (see above), the late-stage variety is also enriched in Sr, Ba and LREE, but poorer in HREE [$(La/Yb)_{cn}$ = 0.22±0.02 and 207±30, respectively; Fig. 3a]. As can be expected (see above), the Eu/Eu* and Eu/Sr ratios are lower in the late-stage crystals relative to the hydrothermal calcite: 0.88±0.04 vs. 1.3±0.1 and 0.0035± 0.0012 vs. 0.023±0.001, respectively. The Y/Ho values in the late-stage variety are higher than normal (on average, 34±1), but lower than in the hydrothermally reworked samples described above.

Trace elements in carbonatitic calcite: a synthesis of published and new data

In this work, the highest levels of REE and light lanthanides (1837 and 1685 ppm, respectively) were detected in calcite from the Aley carbonatites, which were affected by late-stage dolomitization (Fig. 1e) and accompanied by a zone of fenitization. On the basis of this textural evidence and its high MgO and SrO contents (~1 wt.%), this calcite is interpreted as primary. However, about 98 % of our analyses contain ≤ 1400 ppm REE. The lowest levels of REE (64–92 ppm) are

observed in the Magnet Cove carbonatite. This sample contains a large proportion of cumulus andradite (Appendix 1), which probably served as an early sink for REE and, in particular, HREE (see below). A comparable range of values has been reported in the literature (Fig. 4a and references cited therein).

Neither the presence of Na, nor the negligible levels of As can explain the incorporation of several hundred to ~2000 ppm REE in the calcite structure (Tables 1, 2 and 3). Where present, the distribution of Na is very erratic (e.g., from < 40 to 2183 ppm in the Kerimasi sample) and does not correlate with any of the elements, clearly suggesting that elevated levels of this element result from minute inclusions (possibly, of nyerereite: Zaitsev 2010). The content of As required to compensate for the presence of 1000–2000 ppm REE in the mineral would be in the range from ~500 to 1000 ppm, i.e. much higher than the measured levels of this element

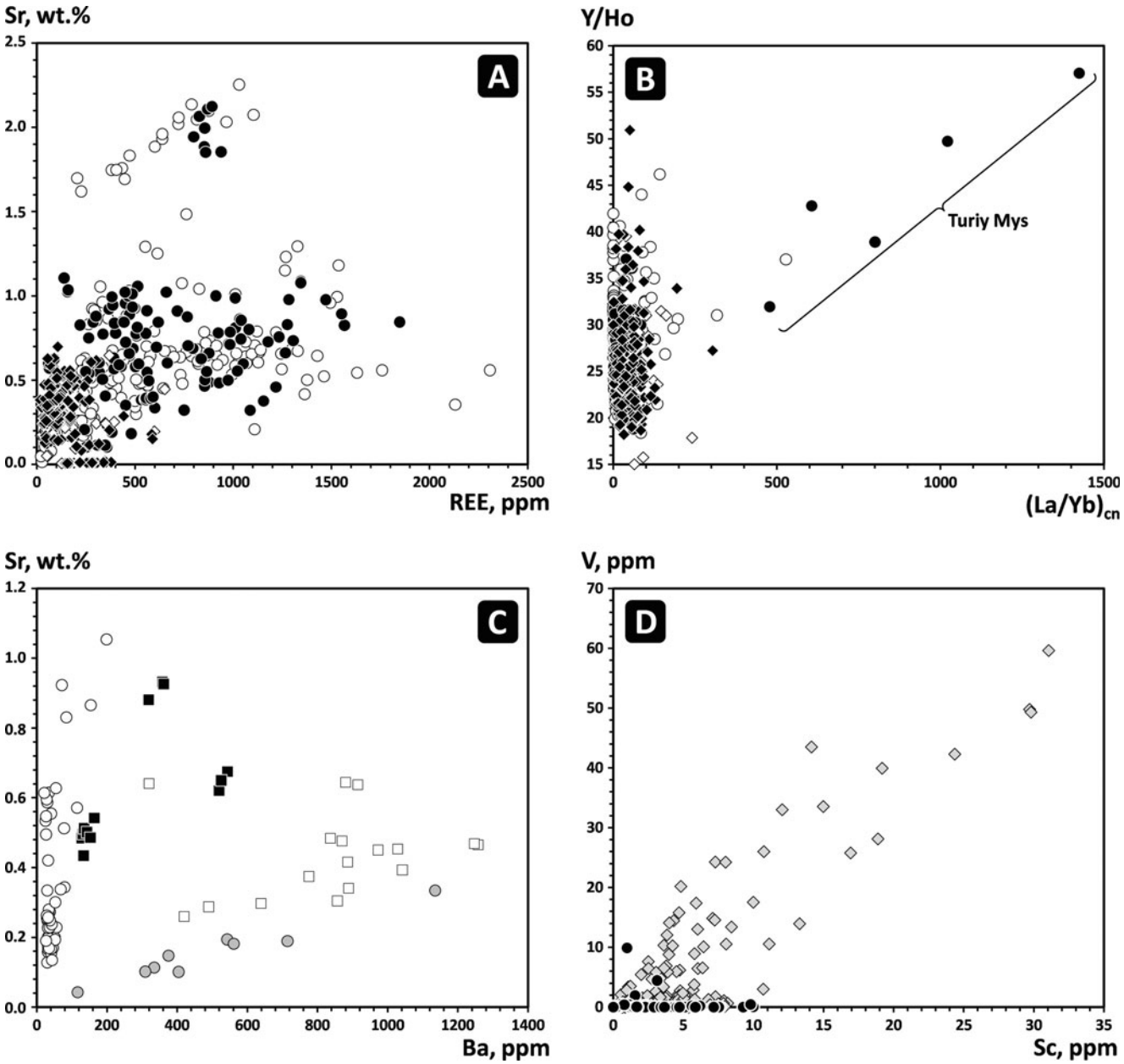

Fig. 4 Trace-element composition of rock-forming carbonate minerals from carbonatites. **a** Sr vs. REE contents in calcite (published data = *empty circles*; this work = *solid circles*) and dolomite (published data = *empty diamonds*; this work = *solid diamonds*). **b** Y/Ho vs $(La/Yb)_{cn}$ values; symbols as in (**a**). **c** Sr vs. Ba contents in calcite from selected localities, including Kerimasi (*grey circles*, this work), Miaoya, China (*empty circles*; Xu et al. 2010), Kovdor, Russia (*solid squares*, Zaitsev et al. 2014) and Darai Piez, Tajikistan (*empty squares*, Faiziev and Gafurov 2010). **d** V vs. Sc contents in calcite (*solid circles*) and dolomite (*grey diamonds*) from Aley (this work). In addition to the publications cited above, diagrams (**a**) and (**b**) were constructed the data from Hornig-Kjarsgaard (1998), Ionov and Harmer (2002), Dawson and Hinton (2003), Xu et al. (2007, 2008a, b)

(Table 2). The equivalent content of P would be about twice as low, but above the detection limit of WDS (~0.03 wt.% P_2O_5). That none of the examined calcite, including the most REE-rich Aley samples, yielded detectable P implies that this element does not play any significant role in REE uptake. Experimental evidence presented in the literature also indicates that P occurs as adsorbed phosphate species (Xu et al. 2014), whose bulk compositional effect is likely negligible. A careful analysis of P distribution in REE-rich calcite by mass-spectrometry and X-ray spectroscopy is needed to resolve these issues.

The patterns of REE distribution normalized to the chondrite composition (Fig. 3a) vary from extremely steep negatively sloping with a high $(La/Yb)_{cn}$ ratio (up to 1742 in the Turiy Mys material) to nearly flat (0.9–5.0 in the Cinder Lake calcite). The former type of patterns is predominant among the samples examined in the present work, i.e. ~70 % of the analyses give $(La/Yb)_{cn} \geq 25$. The dataset of published calcite analyses contains a large proportion of data for (post)orogenic Chinese carbonatites characterized by very low $(La/Yb)_{cn}$ ratios ranging from 0.5 to 2.8 at Miaoya (Xu et al. 2010) to 17–29 at Maoniuping (Xu et al. 2008a). If the number of localities, rather than the number of analyses, is taken into account, about 50 % of the calcite compositions are strongly dominated by LREE. Positive correlation between $(La/Yb)_{cn}$ and REE, clearly expressed in the Aley carbonatites (Fig. 2d), has been previously noted in samples from Kovdor (Zaitsev et al. 2014) and appear to be also present in calcite from Huayangchuan and Shaxiongdong, China (Xu et al. 2007, 2008b). Most of the published data, however, are limited to a single sample and thus, cannot be used to track variations in REE budget across a series of genetically related rocks. Based on the available petrographic evidence, we interpret the Aley trend to result from preferential partitioning of REE into fractionating fluorapatite, which is abundant at Aley and locally forms cumulate units associated with the carbonatites (Chakhmouradian et al. 2015b). The greater affinity of fluorapatite for LREE relative to heavy lanthanides and Y (Dawson and Hinton 2003) drives the composition of carbonates to progressively lower $(La/Yb)_{cn}$ ratios, which explains the correlation seen in Fig. 2d. Early crystallization of other minerals capable of scavenging REE will change the vector of geochemical evolution, as exemplified by the compositions from monazite-bearing sample AL3A (Table 3). Monazite separates LREE from HREE much more efficiently than fluorapatite, which results in a greater change in $(La/Yb)_{cn}$ value for the same drop in REE (Fig. 2d). Hypothetically, fractionation of monazite alone or LREE fluorocarbonates, for example, will yield an even steeper trend with respect to the $(La/Yb)_{cn}$ axis, probably similar to the distribution shown by the Aley dolomite (see below).

Even if we exclude the large Aley dataset, the absolute majority of published and unpublished analyses (84 %) give a Y/Ho ratio of 18–34, with a median value of 30, i.e. close to the Aley average of 27.0±1.8. The Turiy Mys sample yielded the highest Y/Ho ratios measured in carbonatitic calcite to date (49–57), which correlate with its extreme enrichment in LREE relative to HREE (Figs. 3a and 4b). Hydrothermally modified calcite from Bear Lodge also shows elevated Y/Ho values (39–41), but is characterized by depletion in LREE and a small positive Eu anomaly ($Eu/Eu^* = 1.3 \pm 0.1$). The two samples also differ in abundances of large-ion lithophile elements (Table 3), as described above. Analysis of the literature suggests that the Turiy Mys and Bear Lodge compositions represent two extreme cases of trace-element fractionation associated with hydrothermal reworking of igneous carbonates. The differences between the two samples clearly arise from variations in the chemistry of carbonatitic fluids and their ability to mobilize and fractionate REE, Sr, Ba and Pb. The low levels of LREE, Sr and Ba in the Bear Lodge material stem from the preferential partitioning of these elements into hydrothermal ancylite, LREE fluorocarbonates, strontianite and barite, which are common throughout this deposit (Moore et al. 2015), but were not observed in the Turiy Mys carbonatite. Physicochemical parameters, which are most likely to control the nature of hydrothermal Sr-Ba-REE mineralization and, thus, also the composition of cogenetic rock-forming carbonates, include $a(F^-)$, $P(CO_2)$ and pH.

The Mn content of carbonatitic calcite varies from nil to several thousand ppm among the studied samples; the majority of published and new data fall in the 500–5000 ppm range. Unusually low levels of this element (<100 ppm) were observed in the samples from Kerimasi, Magnet Cove and Bear Lodge, all of which also exhibit some Ce deficiency with respect to the values calculated by interpolation from La and Pr. The strong Ce anomaly in the supergene calcite from Bear Lodge and its extreme depletion in Mn undoubtedly resulted from the oxidation of Mn and Ce and their sequestration in Mn^{3+}-Mn^{4+} oxides and cerianite abundant in the host laterite (Moore et al. 2015). The reasons for the low Mn contents (<82 ppm) and Ce/Ce* ratios in the Kerimasi and Magnet Cove samples (0.58±0.15 and 0.47±0.04, respectively) are less clear. Although it is tempting to tie these compositional features in with an increase in O_2 fugacity owing to shallow emplacement of the parental magma and "loss" of some of the Mn and Ce to oxidation, there is no sufficient petrographic or mineralogical evidence to support such an interpretation. Cerianite and Mn^{3+}-bearing spinel-group minerals have been documented at the Kerimasi paleovolcano (Reguir et al. 2008; Zaitsev et al. 2011), but not at Magnet Cove, which has been known for at least 170 years and is reasonably well studied. Zircon could serve as an alternative host for Ce^{4+} (Thomas et al. 2002), but the REE distribution in zircon from neither of these localities has been analyzed. Alternatively, the "exponential" chondrite-normalized REE pattern exhibited by the Kerimasi and Magnet Cove calcite could be merely a reflection of the preferential removal of HREE and

progressively smaller proportions of larger lanthanides from the melt by calcic garnets, which do typically exhibit normalized profiles complementary to that marked "MC" in Fig. 3a, i.e. showing a steep positive slope between La and Nd and flattening out beyond Sm (e.g., Marks et al. 2008). It is noteworthy that the data for calcite from the Oka carbonatite in Canada (Hornig-Kjarsgaard 1998), which is known for the common occurrence of both Mn-rich magnetite and calcic garnet, also give low Ce/Ce* values (0.39–0.86). A detailed study of carbonatites containing garnets, cerianite, zircon and Mn-rich spinels is currently underway to constrain the effect of these minerals on magma evolution and the chemistry of rock-forming carbonates.

The Sr and Ba concentrations measured in the present work are well within the limits established in previous studies (Tables 1, 2 and 3). The highest levels of these elements have been reported in the so-called "strontium-barium" carbonatites from Sarnu Dandali, India, and Murun, Siberia (Wall et al. 1993; Konev et al. 1996), where calcite formed by exsolution of complex Ca-Sr-Ba carbonates. High Sr and Ba contents were also measured in calcite from the Bearpaw Mts., Montana, strongly affected by subsolidus processes (Chakhmouradian et al. 2015a). Several samples from the present work and the literature show a positive correlation between the abundances of Ba and Pb (e.g., Aley; Fig. 2b), or Ba and Sr (e.g., Kerimasi; Fig. 4c), but the rest of the data show converging trends or more complex relationships among these elements (see Kovdor in Fig. 4c), suggesting that their distribution in rock-forming carbonates could be affected by crystal fractionation of two or more different phases. Unfortunately, the available information is insufficient to determine with certainty what minerals can produce concerted depletion of the magma in large-ion lithophile elements. Among those commonly occurring in carbonatites, fluorapatite contains appreciable Sr and Ba and could account for the Sr-Ba trend observed in the Kerimasi calcite, for example, but Pb levels in this mineral are too low (<15 ppm; authors' unpublished data) to cause the one-order-of-magnitude Pb depletion in the Aley rocks (Fig. 2b and f). Theoretically, early-crystallizing pyrochlores, phlogopite or barite-group sulfates could be an alternative host for Sr, Ba and Pb, but trace-element data available for these minerals are scarce (Reguir et al. 2009; Chakhmouradian et al. 2015b).

The highest Pb contents, far exceeding those reported in the literature (≤139 ppm: Xu et al. 2007), were observed in the late-stage calcite from Bear Lodge, whose analyses also gave unusually high U values (see above). It is plausible that the highly oxidizing environment, where these crystals formed, was somehow responsible for their anomalous enrichment in Pb and U, but the mechanism of this enrichment remains to be determined. Increased availability of Pb^{2+} can be explained by the oxidation of galena at Eh levels too low to stabilize Pb^{4+} (<0.8 V: Reeder et al. 2006). In the range of conditions where both CeO_2 and Pb carbonates are stable (i.e., Eh > 0 and mildly alkaline pH), U is oxidized and forms uranyl-carbonate complexes (Ondruš et al. 2003), suggesting that $(UO_2)^{2+}$ is more readily incorporated in calcite than U^{4+} prevalent in the igneous environment. This conclusion is consistent with high concentrations of structurally bound U^{6+} in some sedimentary calcite (Kelly et al. 2006).

Trace elements in carbonatitic dolomite: a synthesis of published and new data

Many of the above arguments regarding the incorporation of REE are also applicable to dolomite. The highest REE contents reported in the literature are close to 600 ppm (Hornig-Kjarsgaard 1998; Chakhmouradian et al. 2009), whereas in the present work, the most REE-enriched compositions correspond to the products of calcite dolomitization at Aley (Table 4). The limited published data (Dawson and Hinton 2003; Zaitsev et al. 2014) and our own results show that dolomite is appreciably poorer in REE relative to cogenetic calcite from the same locality (Figs. 2d and 3d). The published analyses lack Na, As or P values, whereas our LA-ICP-MS measurements show insufficient Na and As to charge-balance the observed REE concentrations, but the critical P data are limited to WDS analyses (Table 2). Thus, the charge-compensation mechanism operating in REE-rich dolomite also remains unclear. The chondrite-normalized patterns of REE distribution range from negatively sloping LREE-enriched to flat in the LREE range, but sloping either down (prevalent type) or up toward HREE (Fig. 3d). The published and new analyses cover a $(La/Yb)_{cn}$ range of 0.3 to 303, but some 83 % of the data fall within a much smaller range (20–150).

Table 5 Primary calcite and dolomite in carbonatites: selected element ratios

Calcite, $CaCO_3$		
Ratio	Average ± ESD or range	No. of analyses/localities
Mg/Mn	0.03–30	174/18
Eu/Eu[a]	1.01±0.14	264/21
Ce/Ce[a]	0.99±0.09	279/22
Eu/Sr	0.0013±0.0011	295/24
Y/Ho	30±8	293/24
$(La/Yb)_{cn}$	0.5–528	283/23
Dolomite, $Ca(Mg_{1-x}Fe_x)(CO_3)_2$ ($x<0.5$)[a]		
Ratio	Average ± ESD or range	No. of analyses/localities
Eu/Eu[a]	1.00±0.17	186/7
Ce/Ce[a]	0.99±0.09	221/8
Eu/Sr	0.00030±0.00035	213/7
Y/Ho	25±6	220/8
$(La/Yb)_{cn}$	0.8–303	217/8

[a] Compositions containing > 50 mol% $CaFe(CO_3)_2$ were not studied in the present work

Although the trend seen in Figs. 2d could results from fractionation of monazite or another LREE-rich mineral, as discussed above, we also cannot rule out the possibility that partitioning of REE between fluorapatite and its parental melt could be very different in magmas that produce dolomite and calcite carbonatites. If present, such variations would give a variety of REE depletion trends depending on the Ca/Mg ratio in the melt.

As can be expected from the structural differences between calcite and dolomite (Table 1), the latter mineral has a greater capacity for small cations approaching Mg^{2+} in ionic radius (0.72 Å: Shannon 1976). Indeed, carbonatitic dolomite is higher in Sc (0.745 Å), V (0.64 Å) and Mn (0.83 Å) than calcite (Table 2; Fig. 4d). The consistently lower Sr, Ba and Pb levels in the dolomite analyses (Figs. 2b and 4a), however, are counterintuitive because the Ca site in the dolomite structure is 2–3 % larger than in calcite (Markgraf and Reeder 1985; Reeder and Dollase 1989). Under equilibrium, synthetic calcite and dolomite have comparable Sr contents (Brice and Chang 1973). There are three possible explanations for this

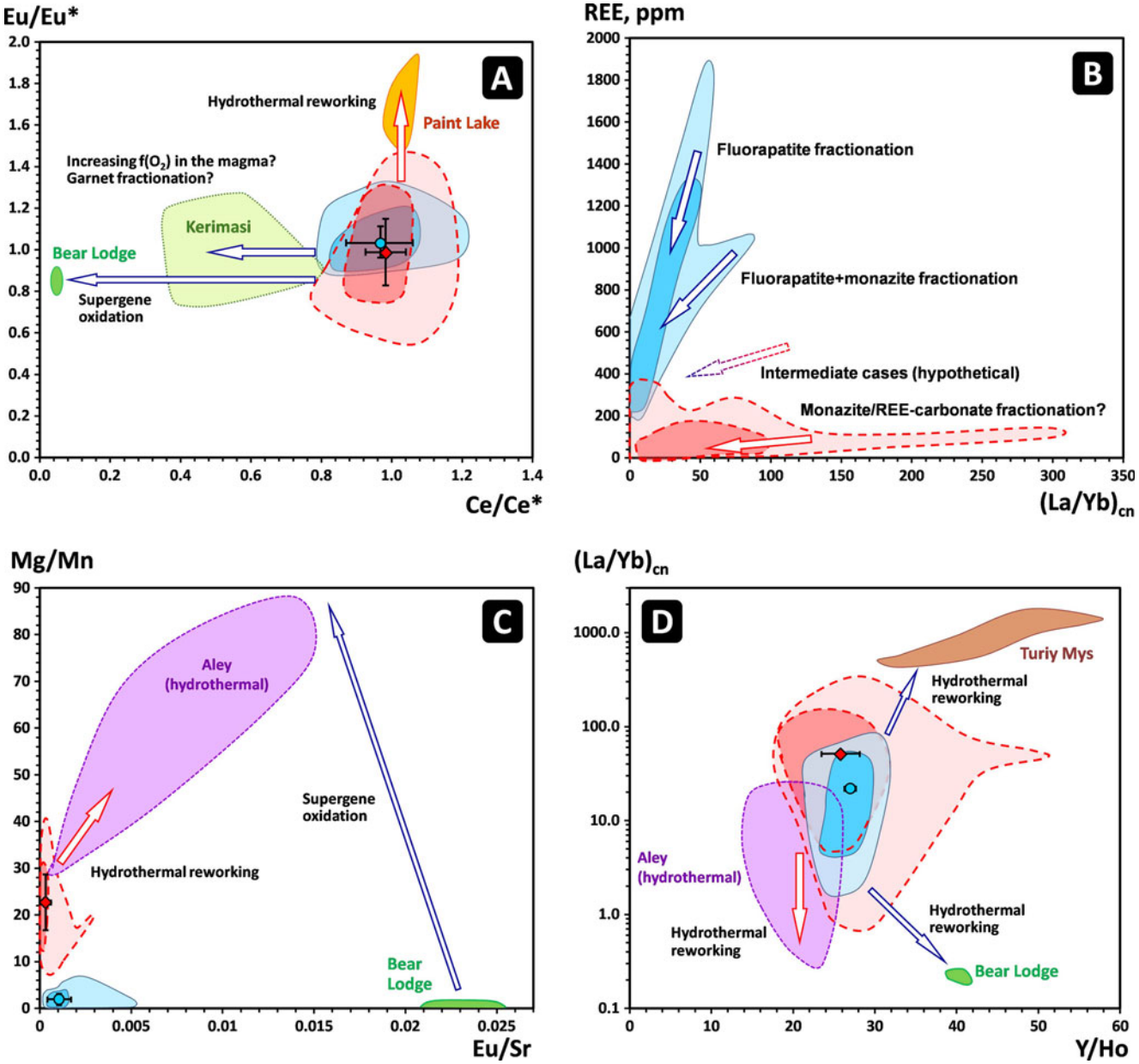

Fig. 5 The extent of trace-element variation in primary calcite and dolomite (as exemplified by 55 samples from the Aley complex) and trends of compositional evolution of rock-forming carbonates identified at Aley and other localities. Fields comprising all of the Aley data points are *shaded pale blue* (calcite, n=75) and *pink* (dolomite, n=170); fields incorporating 80 % of the data are *shaded blue* and *red*, respectively. Mean values (± one standard deviation) are shown, where applicable, as *blue circles* (calcite) and *red diamonds* (dolomite). Other compositional fields (all data from this work) and inferred compositional evolution trends (*blue* for calcite, red for dolomite) are labeled individually

discrepancy: (1) dolomite carbonatites derive from magmas impoverished in Sr, Ba and Pb relative to their calcite counterparts; (2) competition from other minerals more efficient at scavenging large-ion lithophile elements than dolomite; and (3) partitioning of these elements between calcite or dolomite and a carbonate melt differs significantly from experimental results based on solid-state reactions. Low levels of Sr, Ba and Pb in the magma (mechanism 1) may be a primary signature inherited from its source, or an outcome of magma evolution. For example, early fractionation of calcite or fluorapatite from a mantle-derived dolomitic melt could have this type of depleting effect. In the case of Aley, this model is supported by geochemical and petrographic evidence (Chakhmouradian et al. 2015b), and the distribution of data in Fig. 2a and b can be interpreted as a fractionation trend. Conversely, calculations of Dawson and Hinton (2003) for cogenetic dolomite and calcite from Phalaborwa (Palabora), South Africa, suggest that all three elements of concern partition strongly into the latter mineral in order of decreasing ionic radius: $D_{Ba} > D_{Pb} > D_{Sr}$. Further study of trace-element distribution in carbonates from genetically related rock series is required to assess the relative importance of each of the three hypothetical mechanisms proposed above.

Conclusions

Despite their extensive variation in the content of individual trace elements (Tables 1, 2, 3 and 4; Figs. 2, 3 and 4), calcite and dolomite from carbonatites exhibit fairly consistent ratios between some of the elements, especially those sensitive to redox conditions (Table 5). The Y/Ho value, controlled by cation complexation in aqueous systems or volatile-rich melts (Bau 1996; Bühn et al. 2003), is somewhat less consistent (Fig. 4b), but in common with the redox-sensitive parameters, is typically within the error of the chondrite and primitive-mantle values. $(La/Yb)_{cn}$ values are extremely variable in primary carbonates and, along with their REE content, depend on the nature and extent of magma differentiation preceding the crystallization of calcite or dolomite (Fig. 2d). These processes (possibly, involving fractionation of calcic garnets, or spinel-group minerals and cerianite in oxidized systems) are also capable of yielding Mn- and Ce-deficient calcite documented in some carbonatites. Although the Mg/Mn ratio is sensitive to oxidation and can, in principle, be used as a petrogenetic indicator (e.g., Fig. 3c), it will undoubtedly respond also to the precipitation of magnetite, phlogopite and other ferromagnesian minerals, and this response may not be calculable in mineralogically complex systems. Postmagmatic evolution of carbonatites, involving primarily their interaction with hydrothermal and supergene fluids, generates significant changes in the trace-element composition of rock-forming carbonates; however, the same type of process can sometimes produce dramatically different results. For example, hydrothermal alteration can generate either enrichment or depletion in LREE and large-ion lithophile elements, depending on physicochemical variations that are poorly constrained at present. The major conclusions of this work are best summarized in a series of diagrams, where the typical range of primary compositions is delineated by the extensive analytical datasets representing the Aley carbonatites, and the effects of different evolutionary processes are shown as schematic trends (Fig. 5). Systematic studies of other composite intrusions incorporating products of protracted magma evolution and various postemplacement processes (hydrothermal reworking, deformation, metamorphism, weathering) will be essential to developing an integrated geochemical model of carbonatite evolution.

Acknowledgments This work was supported by the Natural Sciences and Engineering Research Council of Canada (NSERC) and Manitoba Geological Survey. The instrumentation used for data collection was supported by the NSERC and Canada Foundation for Innovation. Taseko Mines Ltd. and Jeremy Crozier are gratefully acknowledged for providing us with access to the Aley property and drill core. Meghan Moore and Alexey Rukhlov are thanked for the Bear Lodge and Upper Fir samples, respectively. The material from Kerimasi, Prairie Lake and Magnet Cove was provided by the Natural History Museum (London, UK). The present manuscript has benefited from constructive reviews provided by two anonymous referees.

References

Alexandratos VG, Elzinga EJ, Reeder RJ (2007) Arsenate uptake by calcite: macroscopic and spectroscopic characterization of adsorption and incorporation mechanisms. Geochim Cosmochim Acta 71: 4172–4187

Anders E, Grevesse N (1989) Abundances of the elements: meteoritic and solar. Geochim Cosmochim Acta 53:197–214

Anovitz LM, Essene EJ (1987) Phase equilibria in the system $CaCO_3$–$MgCO_3$–$FeCO_3$. J Petrol 28:389–414

Bau M (1996) Controls on the fractionation of isovalent trace elements in magmatic and aqueous systems: evidence from Y/Ho, Zr/Hf, and lanthanide tetrad effect. Contrib Mineral Petrol 123:323–333

Bau M, Koschinsky A (2009) Oxidative scavenging of cerium on hydrous Fe oxide: evidence from the distribution of rare earth elements and yttrium between Fe oxides and Mn oxides in hydrogenetic ferromanganese crusts. Geochem J 43:37–47

Bose PN (1884) Geology of the Lower Narbadá Valley between Nimáwar and Káwant. Mem Geol Soc India 21:1–72

Brice WR, Chang LLY (1973) Subsolidus phase relations in aragonite-type carbonates. III. The systems $MgCO_3$-$CaCO_3$-$BaCO_3$, $MgCO_3$-$CaCO_3$-$SrCO_3$, and $MgCO_3$-$SrCO_3$-$BaCO_3$. Am Mineral 58: 979–985

Brøgger WC (1921) Die Eruptivgesteine des Kristianiagebietes. IV. Das Fengebiet in Telemark, Norwegen. AW Brøggers Boktrykkeri A/S, Kristiania, 408 pp

Buckley HA, Woolley AR (1990) Carbonates of the magnesite-siderite series from four carbonatite complexes. Mineral Mag 54:413–418

Bühn B, Schneider G, Dulski P, Rankin AH (2003) Fluid-rock interaction during progressive migration of carbonatitic fluids, derived from small-scale trace element and Sr, Pb isotope distribution in hydrothermal fluorite. Geochim Cosmochim Acta 67:4577–4595

Chakhmouradian AR, Zaitsev AN (2012) Rare earth mineralization in igneous rocks: sources and processes. Elements 8:347–353

Chakhmouradian AR, Böhm CO, Demény A, Reguir EP, Hegner E, Creaser RA, Halden NM, Yang P (2009) "Kimberlite" from Wekusko Lake, Manitoba: actually a diamond-indicator-bearing dolomite carbonatite. Lithos 112S:347–357

Chakhmouradian AR, Reguir EP, Kamenetsky VS, Sharygin VV, Golovin AV (2013) Trace-element partitioning in perovskite: implications for the geochemistry of kimberlites and other mantle-derived undersaturated rocks. Chem Geol 353:112–131

Chakhmouradian AR, Reguir EP, Kressall RD, Crozier J, Pisiak L, Sidhu R, Yang P (2015a) Carbonatite-hosted niobium deposit at Aley, northern British Columbia (Canada): Mineralogy, geochemistry and petrogenesis. Ore Geol Rev 64:642–666

Chakhmouradian AR, Reguir EP, Zaitsev AN (2015) Calcite and dolomite in intrusive carbonatites. I. Textural variations. Mineral Petrol (this volume)

Chang LLY, Brice WR (1972) Subsolidus phase relations in aragonite-type carbonates: II. The systems $CaCO_3$-$SrCO_3$-$PbCO_3$, and $CaCO_3$-$BaCO_3$-$PbCO_3$. Am Mineral 57:165–168

Currie KL, Knutson J, Temby PA (1992) The Mud Tank carbonatite complex, central Australia – an example of metasomatism at mid-crustal levels. Contrib Mineral Petrol 109:326–339

Dawson JB, Hinton RW (2003) Trace-element content and partitioning in calcite, dolomite and apatite in carbonatite, Phalaborwa, South Africa. Mineral Mag 67:921–930

De Capitani C, Peters T (1981) The solvus in the system $MnCO_3$-$CaCO_3$. Contrib Mineral Petrol 76:394–400

Douville E, Charlou JL, Oelkers EH, Bienvenu P, Jove Colon CF, Donval JP, Fouquet Y, Prieur D, Appriou P (2002) The Rainbow vent fluids (36°14′N, MAR): the influence of ultramafic rocks and phase separation on trace metal content in Mid-Atlantic Ridge hydrothermal fluids. Chem Geol 184:37–48

Effenberger H, Mereiter K, Zemann J (1981) Crystal structure refinements of magnesite, calcite, rhodochrosite, siderite, smithonite, and dolomite, with discussion of some aspects of the stereochemistry of calcite type carbonates. Z Krist 156:233–243

Eickmann B, Bach W, Rosner M, Peckmann J (2009) Geochemical constraints on the modes of carbonate precipitation in peridotites from the Logatchev Hydrothermal Vent Field and Gakkel Ridge. Chem Geol 268:97–106

Faiziev AR, Gafurov FG (2010) Trace elements in calcite from the Darai Piez alkaline massif, Central Tajikistan. Geochem Int 48:1254–1258

Grice JD, Van Velthuizen J, Gault RA (2000a) Petersenite-(Ce), a new mineral from Mont Saint-Hilaire, and its structural relationship to other REE carbonates. Can Mineral 32:405–414

Grice JD, Gault RA, Roberts AC, Cooper MA (2000b) Adamsite-(Y), a new sodium-yttrium carbonate mineral species from Mont Saint-Hilaire, Quebec. Can Mineral 38:1457–1466

Högbom AE (1895) Über das Nephelinsyenitgebiet auf der Insel Alnö. Geol Fören Stockh Förh 17(101–158):214–258

Hornig-Kjarsgaard I (1998) Rare earth elements in sövitic carbonatites and their mineral phases. J Petrol 39:2105–2121

Ionov D, Harmer RE (2002) Trace element distribution in calcite-dolomite carbonatites from Spitskop: inferences for differentiation of carbonatite magmas and the origin of carbonates in mantle xenoliths. Earth Planet Sci Lett 198:495–510

Keller J, Zaitsev AN (2006) Calciocarbonatite dykes at Oldoinyo Lengai, Tanzania: the fate of natrocarbonatite. Can Mineral 44:857–876

Kelly SD, Rasbury ET, Chattopadhyay S, Krope AJ, Kemner KM (2006) Evidence of a stable uranyl site in ancient organic-rich calcite. Environ Sci Technol 40:2262–2268

Konev AA, Vorob'ev EI, Lazebnik KA (1996) Mineralogy of the Murun alkaline massif. Siberian Branch Russ Acad Sci, Novosibirsk, Russia, 221 pp (in Russian)

Le Maitre RW (ed) (2002) Igneous rocks: a classification and glossary of terms. Cambridge Univ Press, Cambridge, **236 pp**

Markgraf SA, Reeder RJ (1985) High-temperature structure refinements of calcite and magnesite. Am Mineral 70:590–600

Marks MAW, Coulson IM, Schilling J, Jacob DE, Schmitt AK, Markl G (2008) The effect of titanite and other HFSE-rich mineral (Ti-bearing andradite, zircon, eudialyte) fractionation on the geochemical evolution of silicate melts. Chem Geol 257:153–172

Mitchell RH (2005) Carbonatites and carbonatites and carbonatites. Can Mineral 43:2049–2068

Moore M, Chakhmouradian AR, Mariano AN, Sidhu R (2015) Evolution of rare-earth mineralization in the Bear Lodge carbonatite, Wyoming: mineralogical and isotopic evidence. Ore Geol Rev 64:499–521

Ohta A, Kawabe I (2001) REE(III) adsorption onto Mn dioxide (δ-MnO_2) and fe oxyhydroxide: Ce(III) oxidation by δ-MnO_2. Geochim Cosmochim Acta 65:695–703

Ondruš P, Veselovský P, Gabašová A, Drábek M, Dobeš P, Malý K, Hloušek J, Sejkora J (2003) Ore-forming processes and mineral parageneses of the Jáchymov ore district. J Czech Geol Soc 48:157–192

Reeder RJ, Dollase WA (1989) Structural variation in the dolomite-ankerite solid-solution series: An X-ray, Miissbauer, and TEM study. Am Mineral 74:1159–1167

Reeder RJ, Schoonen MAA, Lanzirotti A (2006) metal speciation and its role in bioaccessibility and bioavailability. Rev Mineral Geochem 64:59–113

Reguir EP, Chakhmouradian AR, Halden NM, Yang P, Zaitsev AN (2008) Early magmatic and reaction-induced trends in magnetite from the carbonatites of Kerimasi, Tanzania. Can Mineral 46:879–900

Reguir EP, Chakhmouradian AR, Halden NM, Malkovets VG, Yang P (2009) Major- and trace-element compositional variation of phlogopite from kimberlites and carbonatites as a petrogenetic indicator. Lithos 112S:372–384

Schweer H, Seidel H (1981) Hochdrucksynthese von Carbonaten. VI. Natrium-Lanthanoid-Carbonate. Z Anorg Allg Chem 177:196–204

Shannon RD (1976) Revised effective ionic radii and systematic studies of interatomic distances in halides and chalcogenides. Acta Crystallogr A32:751–767

Sukheswala RN, Avasia RK (1971) Carbonatite-alkalic complex of Panwad-Kawant, Gujarat, and its bearing on the structural characteristics of the area. Bull Volcanol 35:564–578

Thomas JB, Bodnar RJ, Shimizu N, Shinha AK (2002) Determination of zircon/melt trace element partition coefficients from SIMS analysis of melt inclusions in zircon. Geochim Cosmochim Acta 66: 2887–2901

van Achterbergh E, Ryan CG, Griffin WL (2001) GLITTER on-line interactive data reduction for the LA- ICPMS microprobe. Macquarie Research Ltd, Sydney

Villegas-Jiménez A, Mucci A, Paquette J (2009) Proton/calcium ion exchange behavior of calcite. Phys Chem Chem Phys 11:8895–8912

Wall F, Le Bas MJ, Srivastava RK (1993) Calcite and carbocernaite exsolution and cotectic textures in a Sr, REE-rich carbonatite dyke from Rajasthan, India. Mineral Mag 57:495–513

Wright CW (1915) Geology and ore deposits of Copper Mountain and Kasaan Peninsula, Alaska. US Geol Surv Prof Pap 87:11–110

Xu C, Campbell IH, Allen CM, Huang Z, Qi L, Zhang H, Zhang G (2007) Flat rare earth element patterns as an indicator of cumulate processes in the Lesser Qinling carbonatites, China. Lithos 95:267–278

Xu C, Campbell IH, Allen CM, Chen Y, Huang Z, Qi L, Zhang G, Yan Z (2008a) U-Pb zircon age, geochemical and isotopic characteristics of carbonatite and syenite complexes from the Shaxiongdong, China. Lithos 105:118–128

Xu C, Campbell IH, Kynicky J, Allen CM, Chen Y, Huang Z, Qi L (2008b) Comparison of the Daluxiang and Maoniuping carbonatitic

REE deposits with Bayan Obo REE deposit, China. Lithos 106:12–24

Xu C, Kynicky J, Chakhmouradian AR, Campbell IH, Allen CM (2010) Trace-element modeling of the magmatic evolution of rare-earth-rich carbonatite from the Miaoya deposit, Central China. Lithos 118:145–155

Xu N, Chen M, Zhou K, Wang Y, Yin H, Chen Z (2014) Retention of phosphorus on calcite and dolomite: speciation and modeling. RSC Adv 4:35205–35214

Zaitsev AN (1996) A discussion of carbonatite evolution and nomenclature, and the generation of sodic and potassic fenites. Can Mineral 34:453–468

Zaitsev AN (2010) Nyerereite from calcite carbonatite at the Kerimasi volcano, northern Tanzania. Geol Ore Deposits 52: 630–640

Zaitsev AN, Chakhmouradian AR, Siidra OI, Spratt J, Williams CT, Stanley CJ, Petrov SV, Britvin SN, Polyakova EA (2011) Fluorine-, yttrium- and lanthanide-rich cerianite from carbonatitic rocks of the Kerimasi volcano and surrounding explosion craters, Gregory Rift, northern Tanzania. Mineral Mag 75:2801–2810

Zaitsev AN, Williams CT, Jeffries TE, Strekopytov S, Moutte J, Ivashchenkova OV, Spratt J, Petrov SV, Wall F, Seltmann R, Borozdin AP (2014) Rare earth elements in phoscorites and carbonatites of the Devonian Kola Alkaline Province, Russia: examples from Kovdor, Khibina, Vuoriyarvi and Turiy Mys complexes. Ore Geol Rev 61:204–225

Zhong S, Mucci A (1995) Partitioning of rare earth elements (REEs) between calcite and seawater solutions at 25 °C and 1 atm, and high dissolved REE concentrations. Geochim Cosmochim Acta 59: 443–453